LINC00116 codes for a mitochondrial peptide linking respiration and lipid metabolism

Supplementary materials

Anastasia Chugunova[a,b], Elizaveta Loseva[a], Pavel Mazin[c,d,e], Aleksandra Mitina[c], Tsimafei Navalayeu[a], Dmitry Bilan[f,g], Polina Vishnyakova[h], Maria Marey[h], Anna Golovina[i], Marina Serebryakova[b,i], Philipp Pletnev[a,b], Maria Rubtsova[a,b,i], Waltraud Mair[c], Anna Vanyushkina[c], Philipp Khaitovich[c], Vsevolod Belousov[f,g,j], Mikhail Vysokikh[h,i,1], Petr Sergiev[a,b,i,k,1], and Olga Dontsova[a,b,f,i]

[a]Department of Chemistry, Lomonosov Moscow State University, 119992 Moscow, Russia; [b]Center of Life Sciences, Skolkovo Institute of Science and Technology, Moscow, 143028, Russia; [c]Skoltech Center for Neurobiology and Brain Restoration, Skolkovo Institute of Science and Technology, Moscow, 143028, Russia; [d]Institute for Information Transmission Problems (Kharkevich Institute) RAS, 127051 Moscow, Russia; [e]Faculty of Computer Science, National Research University Higher School of Economics, 119991 Moscow, Russia; [f]Shemyakin-Ovchinnikov Institute of Bioorganic Chemistry, 117997 Moscow, Russia; [g]Pirogov Russian National Research Medical University, 117997 Moscow, Russia; [h]Research Center for Obstetrics, Gynecology and Perinatology, 117198 Moscow, Russia; [i]Belozersky Institute of Physico-Chemical Biology, Lomonosov Moscow State University, 119992 Moscow, Russia; [j]Institute for Cardiovascular Physiology, Georg August University Göttingen, 37073 Göttingen, Germany; and [k]Institute of Functional Genomics, Lomonosov Moscow State University, 119992 Moscow, Russia

[1]To whom correspondence should be addressed.

E-mails: mikhail.vyssokikh@gmail.com (MV) and petya@genebee.msu.ru (PS)

www.pnas.org/cgi/doi/10.1073/pnas.1809105116

Supplementary materials and methods

Plasmid construction

Constructs for gene inactivation and genome editing were created on a basis of pX458 plasmid (1). sgRNA sequences were designed using Feng Zhang lab's server (http://crispr.mit.edu/) and cloned into a pX458 vector according to the Feng Zhang lab's protocol (https://media.addgene.org/cms/filer_public/e6/5a/e65a9ef8-c8ac-4f88-98da-3b7d7960394c/zhang-lab-general-cloning-protocol.pdf) to generate a knockout cell line for 1500011k16Rik. The sequences of the sgRNAs were as follows: sgRNA1: GTGCTGAGTGGTTGCAATGGCGG and sgRNA2: TCGGGCTGCAGCGCGTGCTCAGG.
The full-length cDNA of *1500011k16Rik* and *Cyb5r3* were amplified by PCR with primers (F: 5'-CCATTGATGAGAGCTGTGGC-3'; R: 5'-AGCTAGGGACACACAGGACA-3') and (F: 5'-CAGCGTCCAGCCATCAGAA-3'; R: 5'-CGTCTCTTCTTCGCCACCA-3') correspondingly. Fusions with fluorescent proteins were created by restriction free cloning where cDNA of fluorescent protein were amplified with primers containing complementary sequence to the targeted plasmid and the resulting product was used as a primer itself. eGFP was amplified from the pX458 vector with primers (F: 5'-GCAGGTCGACTCTAGAGGATCCCCTTAGAATTCCTTGTACAGCTCGTCCATG-3'; R: 5'-CCAAGGAGCGATGCTTCACCTTCGTGAGCAAGGGCGAGGAG-3'). All obtained vectors were amplified with primers containing Sfi1 restriction sites and cloned into pSBtet-Neo plasmid (2, 3).

Cell lines

NIH3T3 cells were maintained at 37°C in humidified 5% CO2 in DMEM/F12 medium containing 10% FBS, 1% Penicillin/Streptomycin, and 1% Glutamax. NS0 cells were maintained at 37°C in a humidified 5% CO2 in RPMI 1640 medium supplemented with 10% FBS, 1% Penicillin/Streptomycin, and 1% Glutamax. For knockout generation, cells were transfected with pX458 plasmids by Lipofectamine 3000, according to the manufacturer's protocol. Twenty-four hours after transfections, eGFP positive cells were sorted using Becton Dickinson FACSAria III. As the result we obtained three knockout cell lines with following genotypes (Fig. S2): homozygous ΔMtln-1 (NIH3T3) with full deletion of Mtln ORF; heterozygous ΔMtln-2 (NIH3T3) with full deletion of L116 ORF and big insertion of plasmid DNA (red); heterozygous ΔMtln-3 (NIH3T3) with full deletion of Mtln ORF; homozygous ΔMtln (NS0) with full deletion of Mtln ORF.
Other modified cells were obtained by transposition; they were transfected by plasmids pCMV(CAT)T7-SB100X (2) and pSBtet-Neo (3) with appropriate insertion. Stable cell lines were selected by 7 days growth on geneticin containing media (Thermo Fisher).

Mitochondria isolation

Mitochondria from cultured cells were isolated by differential centrifugation. Firstly, cells were scraped and washed twice in PBS. The cells were pelleted by centrifugation at 500 g for 10 min at 4°C. The cell pellet was suspended in 10x volume of Isolation buffer (0.3 M mannitol, 0.1% BSA, 0.2 mM EDTA, 10 mM HEPES-KOH pH 7.4) and homogenized in loose Dounce-Elvenheim homogenizer for 12 strokes, then a homogenate was centrifuged at 1000g for 10 min at 4°C. Supernatant was collected and spinned at 7,000g for 10 min at 4°C. The resulting pellet, containing crude mitochondria, was suspended in small volume by gentle pipetting and homogenized in tight Dounce-Elvenheim homogenizer for 12 strokes at the same volume ratio of cold Isolation Buffer, final suspension was centrifuged twice at 10,000g for 10 min at 4°C.

Western-blot analysis

Following primary antibodies were used in this study: rabbit polyclonal anti-L116 produced by Eurogentec; rabbit polyclonal anti-Cyb5r3 Santa Cruz Biotech (sc-12040), rabbit polyclonal anti-Tom20 Sigma-Aldrich (HPA011562); goat polyclonal anti-β-actin Abcam (ab8229); rat

monoclonal (3F10) Sigma (11867423001); rabbit polyclonal anti-mCherry Abcam (ab183628); rabbit polyclonal anti-Park7 Abcam (ab18257).
Cells were resuspended in lysis buffer consisting of 100 mM Hepes-KOH pH 7.5, 150 mM NaCl, 0.05% Triton-100X, DTT and complete protease inhibitor cocktail (Roche). Subsequently, protein extracts were separated by SDS-PAGE gel and transferred onto PVDF membrane (GE Healthcare). Membranes were blocked with 5% BSA in TBS buffer containing 0.1% Tween 20 for 1-3 h at room temperature. Incubation with primary antibodies was performed overnight at 4 ºC. Next day, membranes were incubated with appropriate HRP-conjugated secondary antibodies for 1-2 h at room temperature. Using an ECL kit (GE Healthcare), the immunoreactive bands were visualized by a ChemiDoc system (Bio-Rad).

Quantitative RT–PCR
Total RNA was extracted using PureLink RNA kit (Invitrogen). cDNA was synthesized from total RNA using Superscript® reverse transcriptase (Invitrogen). The RT-PCR was performed on individual cDNAs by using SYBR® Green PCR master mix in the CFX96 Touch™ Real-Time PCR Detection System. The primer sequences for *1500011k16Rik*: (F: 5'-CAAGCTGGCAACGACTCA-3'; R: 5'-CTCTCCAGTGCTTTTTATTTTCATCT-3'); for GAPDH: (F: 5'-GGTCCCAGCTTAGGTTCATCAG-3'; R: 5'-GTCGTTGATGGCAACAATCTCCAC-3'). The mRNA expression was calculated by the $2^{-\Delta\Delta CT}$ method and normalized to the expression of GAPDH.

Confocal microscopy
The day before the experiment, cells were seeded into 35 mm glass bottom dishes (MatTek) with 14 mm glass microwell. For mitochondria staining, MitoTracker Green FM (in cells expressing mCherry fusion) and MitoTracker Deep Red FM (in cells expressing eGFP fusion) (Thermo Fisher) diluted in dimethyl sulfoxide, according to manufacturer instructions, were applied at 25 nM final concentration. Cells were analyzed using a Carl Zeiss LSM700 confocal laser microscope equipped with a 63X objective in Opti-Mem without phenol red at room temperature, with excitation/emission wavelengths 480/520 and 610/690 for MitoTracker Green FM and MitoTracker Deep Red FM, respectively.

Flow cytometry measurement of ROS production
Monitoring of ROS production in adherent and suspension cells was performed according to the protocol proposed by Wojtala and colleagues (4). All procedures were conducted in Modified Krebs Ringer Buffer (35 мM NaCl, 5 мM KCl, 1mM $CaCl_2$, 0.4 mM KH_2PO_4, 1 mM $MgSO_4$, 5 mM D-glucose, 20 mM HEPES, pH 7.4). Briefly, after collection, cells were washed twice in buffer. Per each assayed condition, $0.5x10^6$ of cells was taken. Then cells were incubated in 20 μM 2′,7′-dichlorofluorescin diacetate (DCFDA; Sigma, USA) solution in the dark at room temperature for 45 minutes, washed twice and analyzed by FACSCalibur (Becton Dickinson, USA): 10^4 cells in each measurement. To dissipate membrane potential with aim to minimize ROS production (5) FCCP (carbonilcyanide p-triflouromethoxyphenylhydrazone; mitochondrial uncoupler, Sigma, USA) was added till 10 nM final concentration prior to DCFDA staining.

Analysis of mitochondrial membrane potential
Fluorescent probe JC-1 was used for measuring mitochondrial membrane potential by flow cytometry according to the standard protocol provided by manufacturer (Thermo Fisher Scientific). Briefly, collected cells (3×10^5 cells/well) were washed once in PBS and incubated in 0.5 ug/ml JC-1 solution at 37°C during 20 minutes. To verify specificity of staining, uncoupler FCCP was added prior to JC-1 staining. Viability of cells was evaluated by flow cytometry using propidium iodide: cells were incubated in 1 ug/ml propidium iodide solution (Live Technologies, USA) for 5 minutes at 37°C. Then cells were washed twice and analyzed by FACSCalibur at medium flow rate.

Measurement of oxygen consumption

Cell suspension or purified mitochondria was placed into oxygraph (Hansatech, UK) chamber filled with respiration medium MIR05 (6) at room temperature. Oxygen consumption linked to different complexes of mitochondrial respiratory chain were assessed exactly as described (7). Malate and glutamate were used for measuring NAD-linked rotenone sensitive respiration on complex I, succinate in presence of rotenone for complex II, duroquinol was reduced as described before directly before experiment and used as an antimycin sensitive substrate for complex III, ascorbate and N,N,N′,N′-tetramethyl-p-phenylenediamine were used for assessing complex IV activity on potassium cyanide sensitive manner. Stepwise control of the ETC-CI linked respiration was assessed by following protocol (8). The second protocol was performed for checking wild type and knockout, complemented with either L116 gene or luciferase gene as a control to estimate the maximal rate of uncoupled respiration measured in the presence of FCCP with titration until maximum rate was reached (0.2 pmoles – each addition) with the addition of 1 µM rotenone at the end. For every measurement 4×10^6 cells or 100 ug of mitochondrial protein were taken.

Analysis of purified mitochondrial complex I activity

Purified mitochondrial complex I enzyme activity was measured using a complex I enzyme activity assay kit according to the manufacturer's instructions (Cat.ab109721, Abcam). Briefly, 100, 200, and 400 ug samples of total mitochondrial protein extract were loaded into the well of microplate coated with complex I capture antibody, and incubated for 3 hours at room temperature. The activity of complex I was measured by NADH to NAD+ oxidation, which was monitored by absorbance at 450 nm. Complex I activity is expressed as the change in absorbance per minute per microgram of protein.

Co-immunoprecipitation

Cells were harvested in lysis buffer consisting of 100 mM Hepes-KOH pH 7.5, 150 mM NaCl, 0.05% Triton-100X, DTT and cOmplete protease inhibitor cocktail (Roche). Extracts were centrifuged and the concentration of supernatant was measured by Bradford assay. Samples were incubated with 100 ul of anti HA-beads suspension (Sigma Aldrich) overnight. Co-immunoprecipitated proteins were washed and eluted with 0.1 M Gly-HCl, pH 2.8.

NADH dehydrogenase activity

Cyb5r3 enzymatic activity was determined in isolated mitochondria in 20 mM phosphate buffer, pH 7.5, 0.2 mM NADH, and 0.2 mM potassium ferricyanide. The reduction of ferricyanide was monitored at 420 nm at 25 ºC for 5 min. Cyb5r3 activity was expressed as the change in absorbance per minute per microgram protein of mitochondria.

Lipidome

L116 knockouts in murine fibroblast NIH3T3 and myeloma NS0 cell lines were analyzed in separate groups. The NIH3T3 group contained 11 wild-type (WT) samples, 8 samples with ΔMtlnL116-1 genotype (2 technical replicates for each of 4 biological replicates), 6 samples with ΔMtlnL116-2 genotype (2 technical replicates for each of 3 biological replicates), and 6 samples with ΔMtlnL116-3 genotype (2 technical replicates for each of 3 biological replicates), for a total of 31 samples. The second, NS0 group contained 6 WT samples and 10 samples with Δ mutation (2 technical replicates for each of 5 biological replicates)—in total, 16 samples.

Additionally, a group of samples containing 4 WT samples from murine fibroblast NIH3T3 cell line were extracted with 4 samples with ΔMtln-3 genotype (mitochondrial peptide Mtln knockout, 3 clone), 4 samples with $\Delta Cyb5r3_{mito}$ genotype (mitochondrial cytochrome b5 reductase 3 knockout), 3 samples with $\Delta Cyb5r3_{mito}$,ΔMtln-1 genotype (mitochondrial peptide Mtln and mitochondrial cytochrome b5 reductase 3 double knockout), 3 samples with $\Delta Cyb5r3_{mito}$,ΔMtln-2 genotype, and 3 samples with $\Delta Cyb5r3_{mito}$+Mtln genotype (mitochondrial cytochrome b5

reductase 3 knockout and mitochondrial peptide Mtln overexpression, transposone construction pSBtetMtln) - in total 21 samples.

Metabolite extraction and UPLC-MS sample preparation: extraction was performed as described in (9). Two consecutive metabolite extractions from cells were performed at 4^{o}C by addition of 800 ul of cold methyl tert-butyl ether and methanol (3:1) mixture, 30 min incubation, followed by sonication for 10 min. After that 560 ul of water and methanol (3:1) mixture was added to the samples, followed by 10 sec vortexing and centrifugation at 4^{o}C at maximum speed for 10 min. This resulted in separation of the solution into two phases: the upper phase (containing organic solvent) was collected and dried in a speedvac.
The resulting pellet was stored at -80 ^{o}C until analysis. For LC-MS the pellet was resuspended in 200 ul of acetonitrile:isopropanol (3:1) solution, shaken on Vortex-Genie 2 shaker for 10 min at 4 ^{o}C, sonicated in BANDELIN Sonorex Super RK 103 H ultrasonic bath with ice for 10 min, and centrifuged at 4^{o}C at maximum speed for 10 min. For UPLC-MS analysis, samples were diluted 1:20 in acetonitrile:isopropanol (3:1) mixture and transferred to glass vials. Pools of the extracts were prepared as quality control samples (QC) for each line containing 20 ul of sample of the corresponding line, and diluted 1:20.
Prior to the lipid samples injection, the system was flushed by injection of the 4 acetonitrile:isopropanol (3:1) mixture aliquots, followed by 4 QC samples to equilibrate the column. The injection order of the complete each sample set was randomized and QCs were injected after every 5th sample (10). Untargeted lipidome profiling was performed in positive ionization mode (11).

Data Processing
In total we acquired 92 raw files with spectra which were converted into .mzXML format in centroided mode using CompassXport software (Bruker Daltonics). All preprocessing and analysis steps were performed on a Skoltech Pardus cluster. To define best parameters for peak picking and alignment of initial parameter optimization, IPO (12) was implemented with the set of QC files from each group separately. With the defined parameters, xcms (13-15) was run followed by CAMERA (16) resulting in a final matrix with the intensities of all lipid features found in the samples. The final matrix for the NIH3T3 line contained ΔMtlnL116-2 mutants, ΔMtlnL116-3 mutants, and NIH3T3 wild-type samples. ΔMtlnL116-1 mutants had much lower intensity of the signal due to lower initial sample concentration, and thus were not considered in the further analysis. The matrix for the NS0 line contained Δ mutants and NS0 wild-type samples. The matrix with the double knockout samples contained NIH3T3 wild-type samples, ΔMtln samples, ΔCyb5r3mito and ΔMtln double knockouts, and ΔCyb5r3 and Mtln overexpression samples. In total, there were 3266, and 3804 and 6393 lipid features detected in NIH3T3, NS0, and double-knockout group respectively. The downstream statistical analysis was done in an R programming environment (17).

Filtration, normalization and analysis
All features with retention time of less than 10 seconds and more than 1200 seconds were removed, assuming that they mostly represent column contamination; 1st and 2nd isotopic peaks were removed, leaving only monoisotopic peaks. This resulted in 1587 and 1881 peaks in the NIH3T3 and NS0 lines respectively. For statistical analysis, intensities of all peaks were normalized by upper quartile, and log2-transformed. Further all peaks were annotated with LIPIDMAPS database (18) and candidates were chosen within 20 ppm mass difference in accordance with the retention time window characteristic for each lipid class. Annotation was resolved up to subclass; we considered NH_4^+ adduct for TAG and DAG species, H^+ and Na^+ for phospholipids and sphingolipids. Annotation was performed for the NIH3T3 group dataset, out of 1587 lipid features, 981 had corresponding hits in the LIPIDMAPS database, 400 features were assigned to a certain class only, and 641 were assigned to a certain lipid category. The NS0 group dataset was then

compared to NIH3T3 results with a maximal mass delta of 0.1 ppm and maximal retention time deviation of 2 sec. There were 957 lipid features comprising dataset 1 (DS1) that matched both groups. Technical replicates were averaged. A T-test with BH-correction for multiple testing was applied to find lipids with significant concentration difference between the wild type and knockout lines. To estimate effect size, log2 fold change (log2FC, difference between mean normalized and log2-transformed intensities) was calculated. Relative intensity was calculated as a fraction of raw intensity and total peak intensity in the given sample, and was used as an estimate of mass fraction. For double knockouts dataset (DS2) only peaks with retention time and mass/charge matched those in DS1 were used. To achieve this, we matched peaks from DS1 to peaks in DS2 with m/z difference lower than 0.1 and with retention time difference below 0.1 minute. With these parameters peaks were matched one-to-one. This procedure allowed us to compare 656 peaks between datasets, only these peaks were used in analysis of DS2. All intensities were log2 transformed and upper-quartile normalized. Means of normalized values were used to calculate log2 fold changes. T-test with Benjamini-Hochberg correction for multiple testing was used for statistical testing.

Imaging NADH/NAD+ in cells using SoNar sensor

The cells were plated into 35-mm glass bottom dishes (SPL life sciences) and cultured under standard conditions. The cells were transfected by a mixture of 1 ng vector DNA (pcDNA3.1-SoNar or pcDNA3.1-iNapC vectors) and 3 ul FuGENE HD transfection reagent (Promega) per dish according to manufacturer recommendations. Twenty-four hours after transfection, the culture medium was changed to a Hanks balanced salts solution (PanEko) supplemented with 20 mM of HEPES KOH pH 7 (PanEko).

Leica DMI 6000 B widefield fluorescent microscope equipped with a HCX PL Apo CS 40.0×1.25 Oil UV objective was used for imaging. Temperature was maintained at 37ºC throughout the period of imaging. We detected fluorescence of transfected cells in two separate channels corresponding to two peaks in the excitation spectrum of the SoNar biosensor (with maxima at 420 and 485 nm) and with emission at 528 nm. For the channel corresponding to excitation at 420 nm, we used the following filters: EFW excitation, 427/10 (CFP); emission, BP 542/27 (YFP). For the second channel we used a GFP filter cube: excitation, BP 470/40; dichromatic mirror 500; emission: BP 525/50. Recording intervals were 10 s. Final time series were analyzed using the ImageJ software.

Data analysis

Gel images were quantified using ImageJ v1.51w. Statistical analyses were performed in Prism 7 v7.00.

Supplementary figures

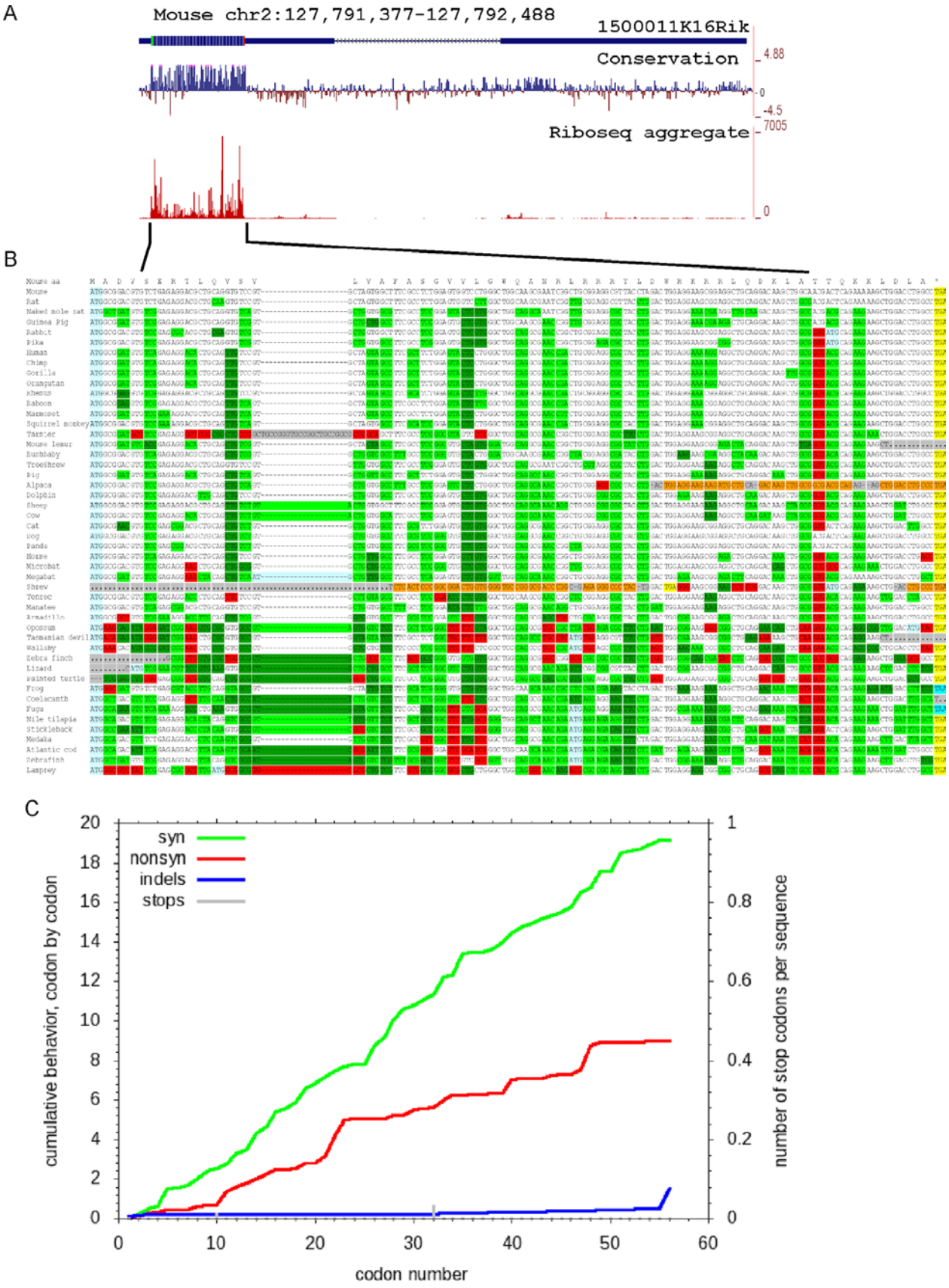

Fig. S1. Analysis of Mtln conservation. (A) Mouse genome area encompassing *1500011k16Rik* gene. Shown are exons and ORF location. Below the map conservation diagram across vertebrates (19) and riboseq coverage diagram are provided (20). (B) Alignment of Mtln coding sequences

across the vertebrates. Colors of the triplets mark synonymous (green), non-synonymous (red), nonsense (yellow) substitutions, and initiation codons (cyan). (C) Cumulative number of synonymous (green), non-synonymous (red), nonsense (grey) substitutions and indels (blue) across the Mtln coding region in vertebrate species.

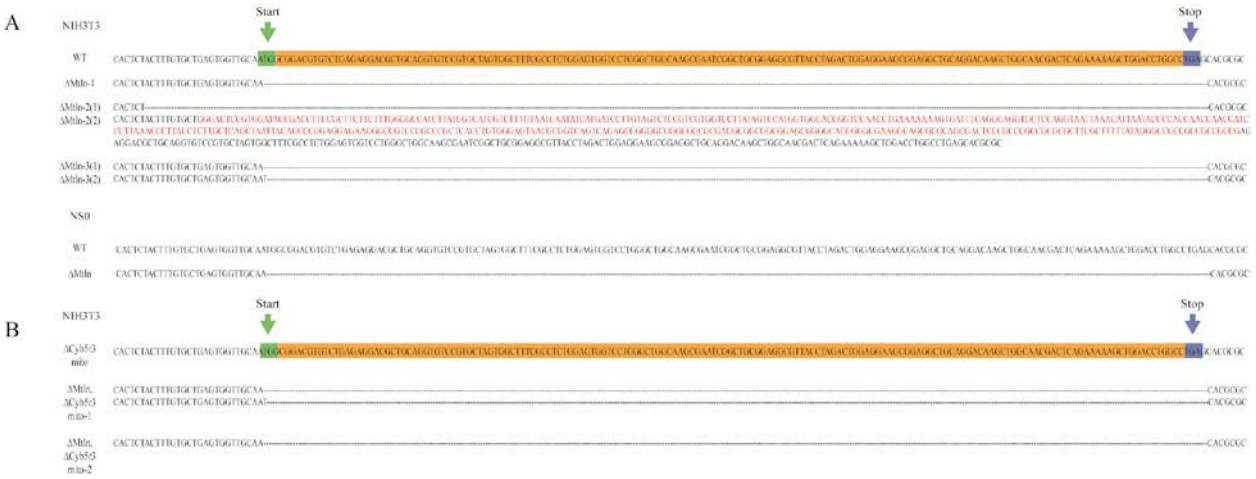

Fig. S2. Inactivation of *1500011k16Rik* gene coding for Mtln. (A) Mouse genome area encompassing *1500011k16Rik* gene in the wild type NIH3T3 and NS0 strains and their derivatives with disrupted Mtln coding area. (B) Mouse genome area encompassing *1500011k16Rik* gene in the Gly2-to-Ala2 Cyb5r3 mutant cell line and its derivatives with disrupted Mtln coding area. Mtln coding area is marked by orange color, start and stop codons are marked by green and blue colors correspondingly. Deleted nucleotides are shown by dashes, spontaneous insertion sequence is shown in red color.

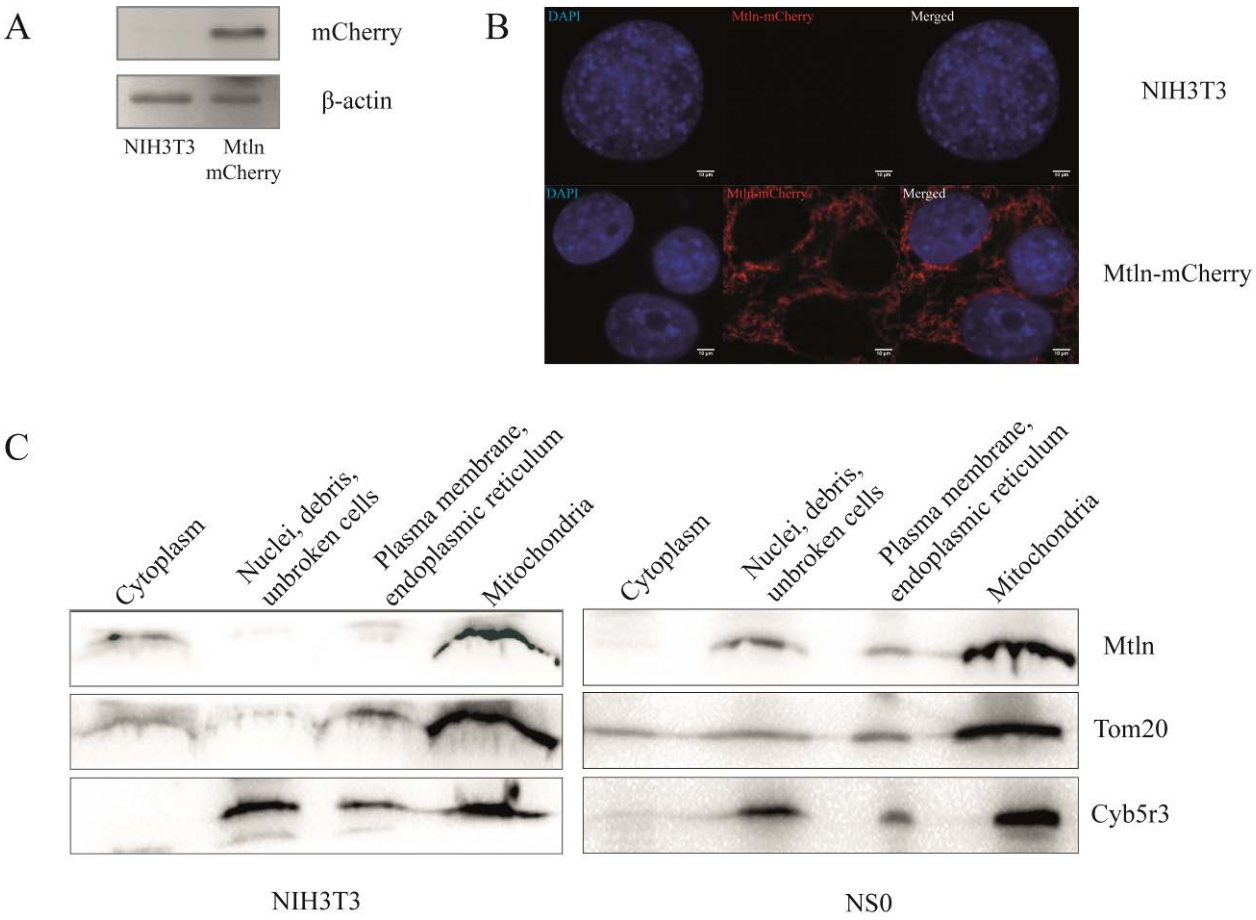

Fig. S3. *1500011k16Rik* encodes a novel polypeptide. (A) Immunoblotting of extracts from NIH3T3 and cells, expressing Mtln-mCherry from natural Mtln promoter, by anti-mCherry antibodies. β-actin was used as a loading control. (B) Immunocytochemistry of NIH3T3 and cells, expressing Mtln-mCherry fusion located in the natural genomic context of Mtln. Nuclei were stained by DAPI. Scale bar is 10 μm. (C) Western-blot analysis of cell fractions by anti-Mtln, anti-Tom20, anti-Cyb5r3 antibodies.

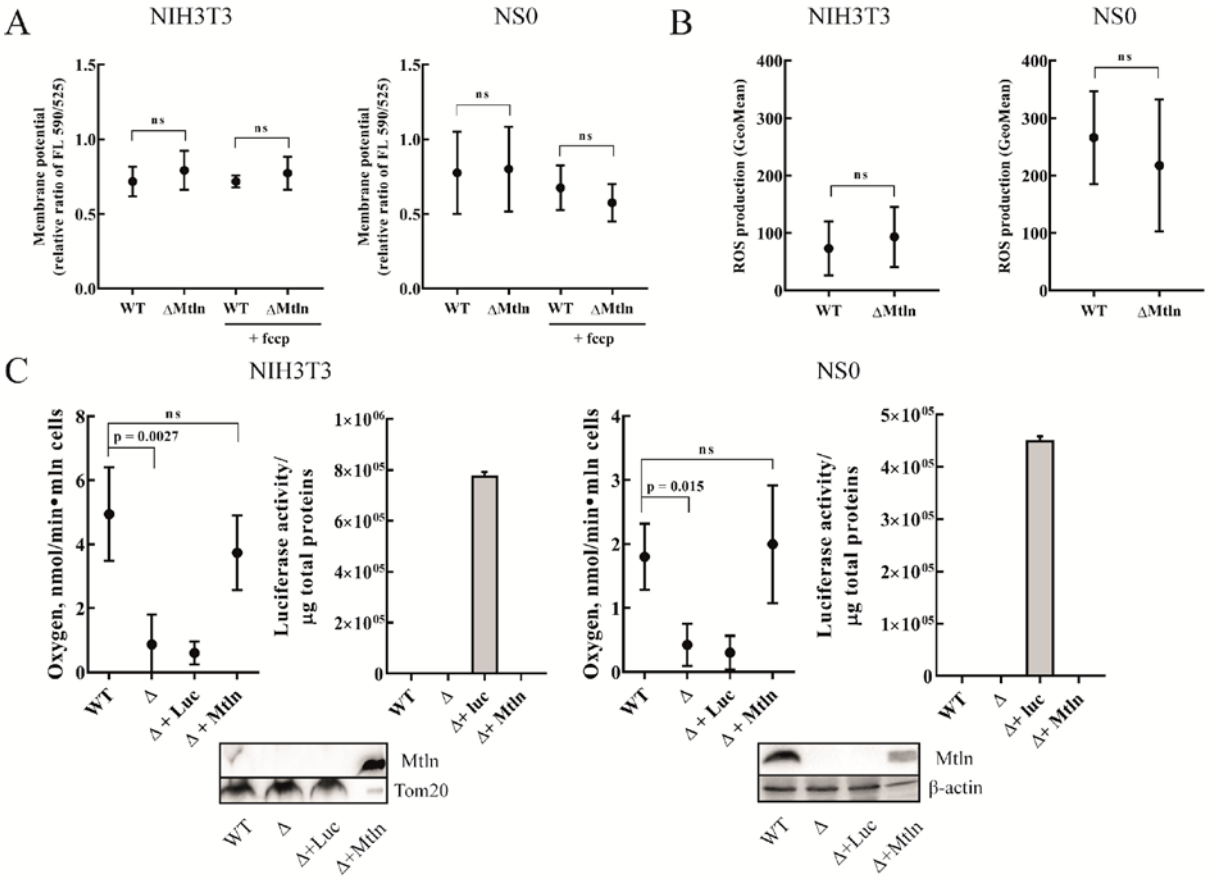

Fig. S4. Mtln inactivation reduces respiratory complex I activity. (A) Mitochondrial membrane potential measured as red to green fluorescence ratio of JC-1 dye localized in mitochondria for the wild type and knockout cell lines (for NIH3T3 ΔMtln6-1,2,3 were measured). Values are average of 6 (for NIH3T3 and 4 for NS0) independent experiments. Student's t-test (ns – not significant). (B) ROS production measured by DCFDA dye in wild type and knockout cell lines (for NIH3T3 ΔMtln-1,2,3 were measured). Values are average of 5 (for NIH3T3 and 4 for NS0) independent experiments. Student's t-test (ns – not significant). (C) Oxygen consumption rates for complex I for parental, knockout, knockout complemented by Luciferase gene and knockout complemented by Mtln gene cell lines (for NIH3T3 only ΔMtln-3 clone was measured). Values are average of 3 independent experiments done in triplicates. For the statistically significant change multiplicity adjusted p-value ($p < 0.05$, One-way ANOVA, Dunnett correction) is indicated. Immunoblotting of isolated mitochondria from NIH3T3 and cell lysates for NS0 show expression of Mtln peptide in these cells. Tom20 was used as a loading control for mitochondria and β-actin for cell lysates. Luciferase assay illustrates the activity only in cells complemented by luciferase. For A, B and C data presented as mean ± SD.

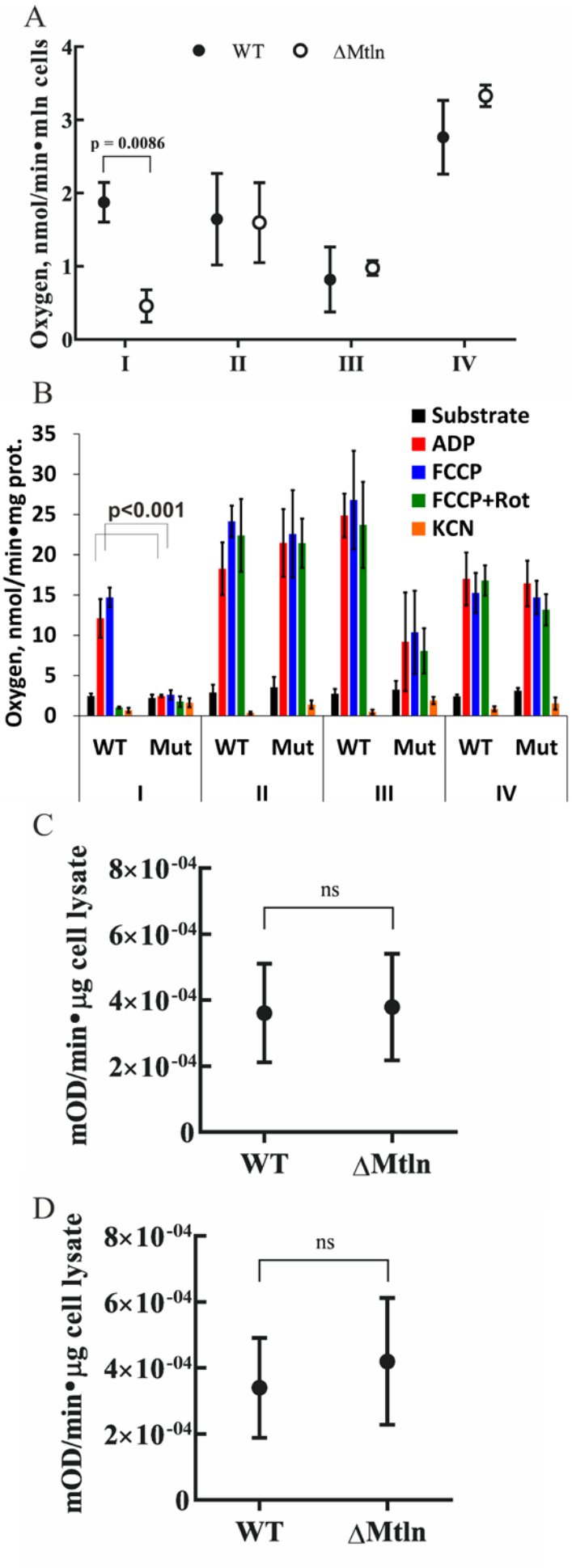
A
WT
ΔMtln
Oxygen, nmol/min•mln cells
p = 0.0086
I
II
III
IV
B
Substrate
ADP
FCCP
FCCP+Rot
KCN
Oxygen, nmol/min•mg prot.
p<0.001
WT
Mut
I
II
III
IV
C
mOD/min•µg cell lysate
ns
WT
ΔMtln
D
mOD/min•µg cell lysate
ns
WT
ΔMtln

Fig. S5. Mtln inactivation reduces respiratory complex I activity. (A) Oxygen consumption rates for complexes I-IV for parental NS0 and ΔMtln cell line. Values are average of 3 independent experiments done in triplicates. For the statistically significant changes multiplicity adjusted p-value ($p < 0.05$, Student's t-test, Holm-Sidak correction) is indicated. (B) Oxygen consumption rates for mitochondria isolated from parental NS0 and ΔMtln cell lines (see Methods for details). Values are average of 3 independent experiments done in triplicates. For the statistically significant changes multiplicity adjusted p-value ($p < 0.05$, Student's t-test) is indicated. (C, D) Activity of isolated complex I in the parental NIH3T3 (C), NS0 (D) and ΔMtln NIH3T3 (C), NS0 (D) cell lines. Values are average of 6 for NIH3T3 and 5 for NS0 independent experiments done in duplicates. Student's t-test (ns – not significant). For A-D data presented as mean ± SD.

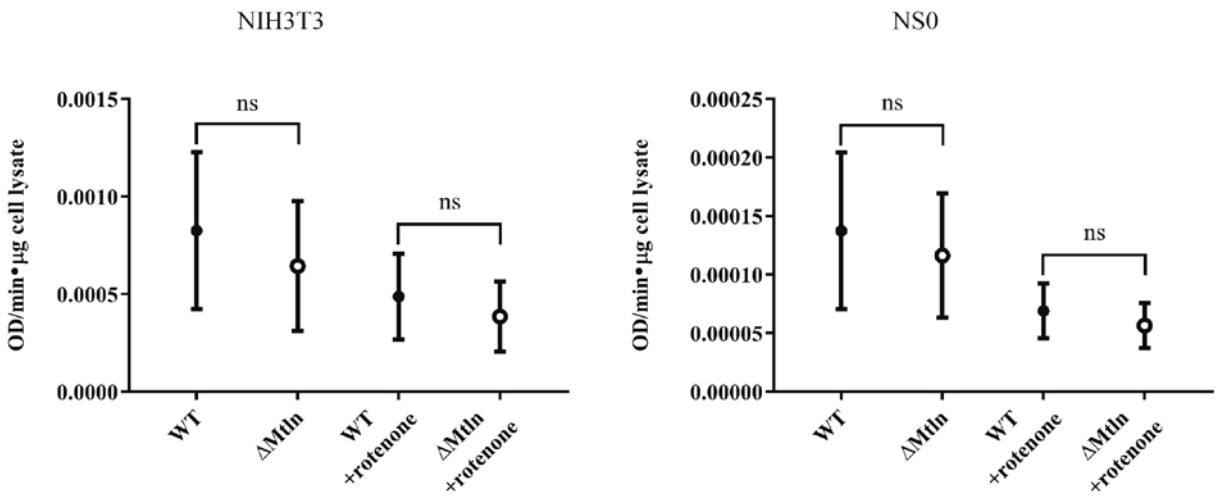

Fig. S6. Mtln inactivation does not affect complex I+III activity. Complex I+III activity measured as NADH dependent cytochrome C reduction in the presence of KCN in isolated mitochondria for wild type and Mtln depleted cells (for NIH3T3 ΔMtln-1,2,3 were measured). Values are average of 4 for NIH3T3 and 3 for NS0 independent experiments done in duplicates. Student's t-test (ns – not significant). Data presented as mean ± SD.

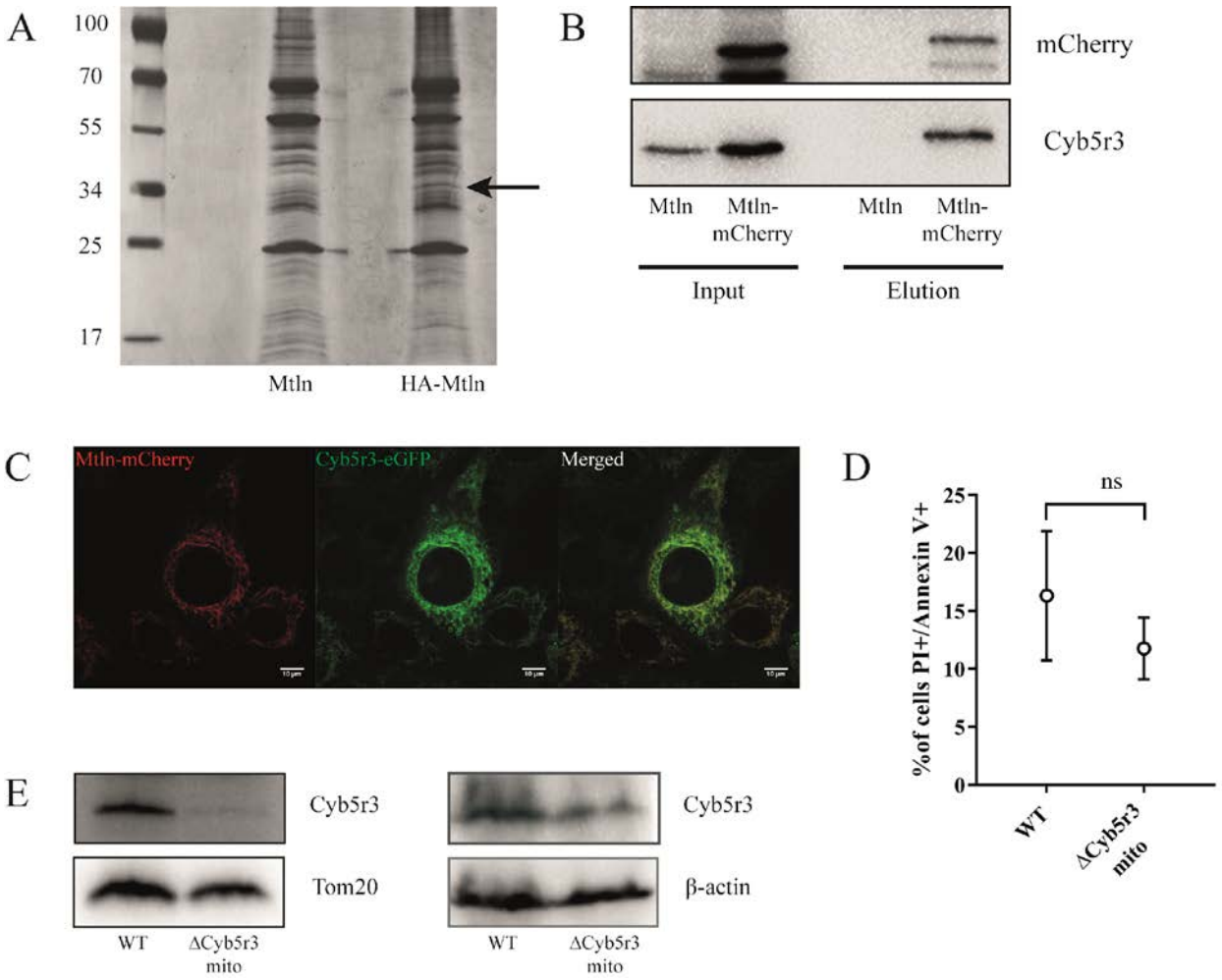

Fig. S7. Mtln interacts with Cyb5r3. (A) Silver staining of the gel with immunoprecipitation of HA-Mtln from NIH3T3. Cells expressing Mtln without the tag were used as a control. (B) Immunoprecipitation of Mtln-mCherry from NIH3T3 cells followed by immunoblotting with anti-mCherry antibodies (top panel) and anti-Cyb5r3 antibodies (bottom panel). Cells expressing Mtln without tag were used as a control. (C) Confocal images of cells expressing mCherry tagged Mtln peptide and eGFP tagged Cyb5r3. Scale bar 10 μm. (D) Analysis of cell viability in NIH3T3 and (Gly2 to Ala2) Cyb5r3 mutant cells. Values are average of 2 independent experiments done in triplicates. Student's t-test (ns – not significant). Data presented as mean ± SD. (E) Western-blot analysis of Cyb5r3 presence in isolated mitochondria (right panel) and whole cell extracts (left panel) from wild type and (Gly2 to Ala2) mutant (ΔCyb5r3$_{mito}$) cells. Tom20 and β-actin were used as a loading control.

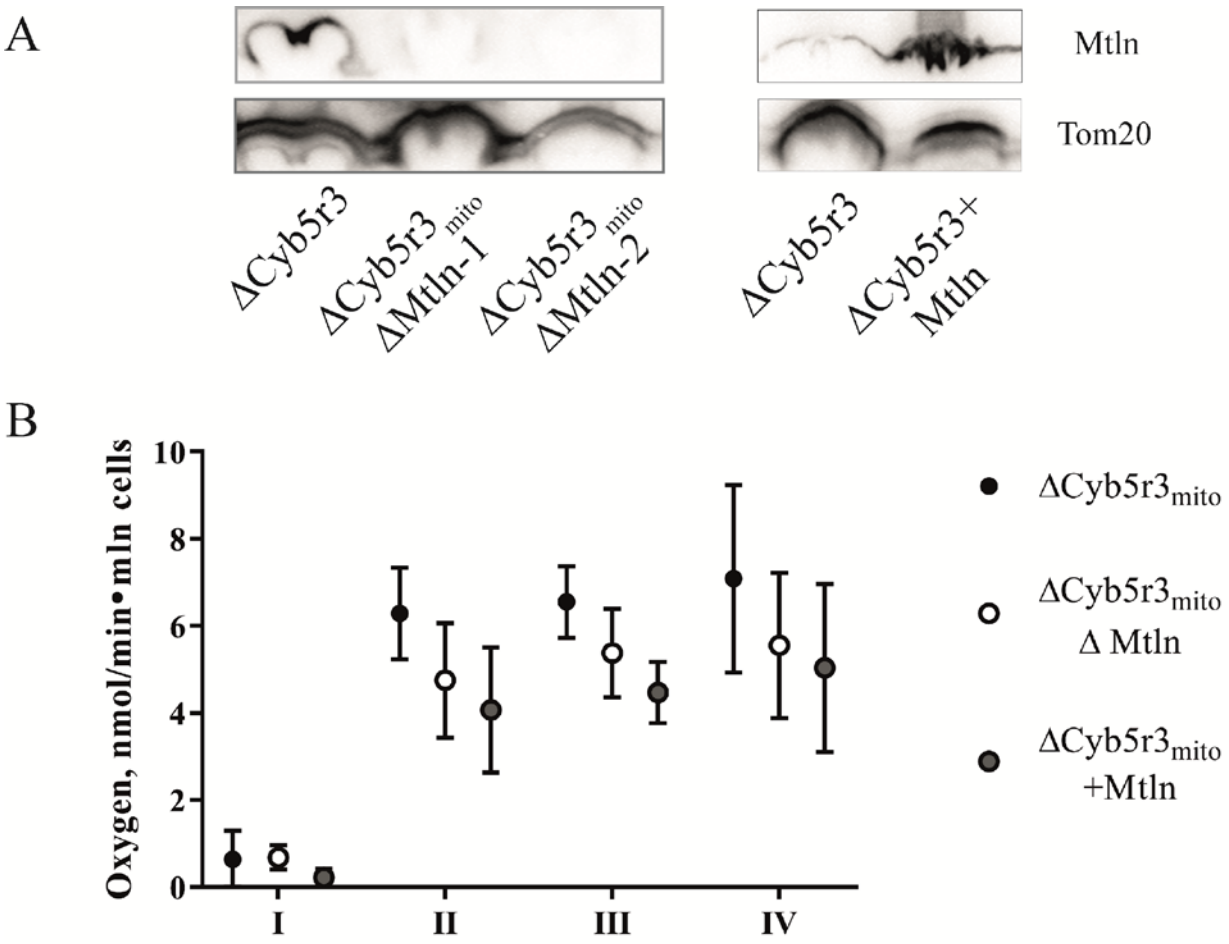

Fig. S8. Mtln knockout and overexpression do not have synthetic respiration phenotype with disruption of Cyb5r3 mitochondrial localization. (A) Western-blot analysis of mitochondrial extracts from (Gly2 to Ala2) Cyb5r3 mutant (ΔCyb5r3$_{mito}$) cell line and its derivatives with Mtln knockout or Mtln overexpression with anti-Mtln antibodies. Tom20 was used as a loading control. (B) Oxygen consumption rates for complexes I-IV for (Gly2 to Ala2) Cyb5r3 mutant cell line (black circles) and its derivatives with Mtln knockout (open circles) or Mtln overexpression (grey circles). For double mutants both ΔCyb5r3$_{mito}$, ΔMtln-1 and ΔCyb5r3 $_{mito}$, ΔMtln-2 clones were measured. Values are average of 3 independent experiments done in triplicates. For the statistically significant changes multiplicity adjusted p-value ($p < 0.05$, Student's t-test, Holm-Sidak correction) was applied. No significant changes were observed.

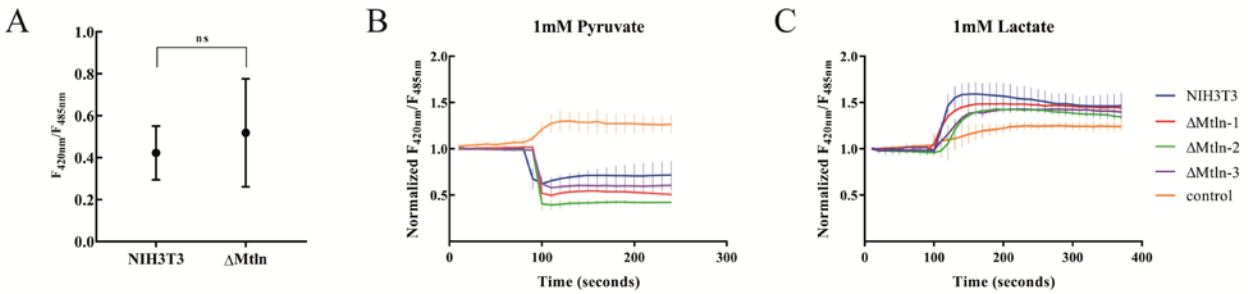

Fig. S9. Mtln does not alter cytosol NADH/NAD$^+$ balance. (A) NADH/NAD+ ratio in Mtln knockout and parental NIH3T3 cell cultures quantified according to SoNar fluorescence. (B) Dynamics of SoNar fluorescence responses in Mtln knockout and parental NIH3T3 cells treated with exogenous 1mM pyruvate. (C) Dynamics of SoNar fluorescence responses in Mtln knockout and parental NIH3T3 cells treated with exogenous 1mM lactate. As a control we used iNapC sensor (72). Values are average of 4 independent experiments. Fluorescence time curves from 20 cells were used for every experiment. Student's t-test (ns – not significant). Data presented as mean ± SD.

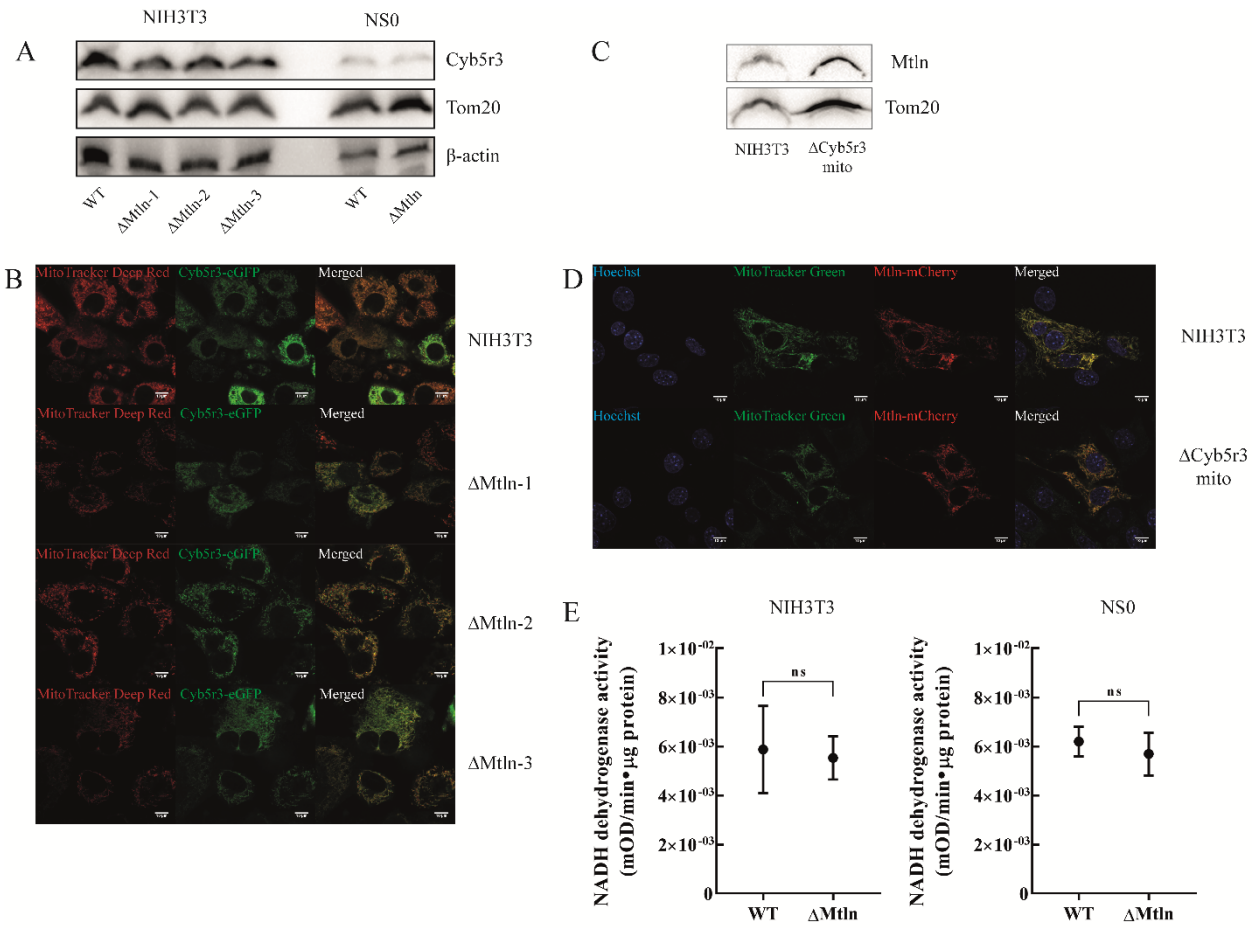

Fig. S10. Mtln do not influence the amount, localization and NADH dehydrogenase activity of Cyb5r3. (A) Western-blot analysis of extracts from the wild type and Mtln knockout cell lines with anti-Cyb5r3 and anti-Tom20 antibodies. β-actin was used as a loading control. (B) Confocal images of NIH3T3 and Mtln knockout cell lines, expressing Cyb5r3-eGFP and stained by MitoTracker Deep Red. Scale bar 10 μm. (C) Western-blot analysis of mitochondrial extracts from the wild type and $\Delta Cyb5r3_{mito}$ mutant cells with anti-Cyb5r3 antibodies. Tom20 was used as a loading control. (D) Confocal images of NIH3T3 and $\Delta Cyb5r3_{mito}$ mutant cells, expressing Mtln-mCherry and stained by MitoTracker Green. Nuclei were stained by Hoechst 33342. Scale bar 10 μm. (E) NADH dehydrogenase activity measured by ferricyanide reduction in parental and L116 knockout cell lines (for NIH3T3 ΔMtln -1,2,3 were measured). Values are average of 4 (for NIH3T3 and 3 for NS0) independent experiments done in duplicates. Student's t-test (ns – not significant). Data presented as mean ± SD.

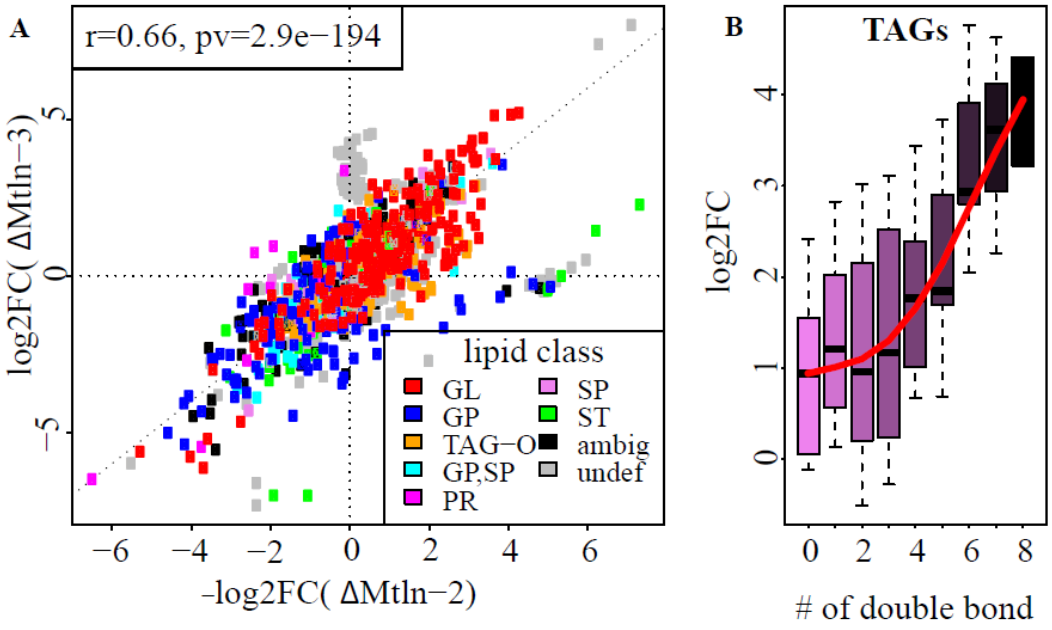

Fig. S11. Mtln depletion alters level of phospholipids and triglycerides. (A) Correlation of log2 fold changes observed in NIH3T3 cell line in ΔMtln-2 and ΔMtln-3 genotypes. Different numbers denote different lipid classes: GL - glycerolipids, GP – glycerophospholipids, TAG-O - 1-alkyl-2,3-acylglycerols, SP - sphingolipids, PR - prenol lipids, SP - sphingolipids, ST - sterol lipids. Lipids whose abundance is significantly changed in both Mtln knockout cell lines are shown by filled circles. Pearson correlation coefficient (r) and its p-value (t-test) for all lipids and for lipids with significant changes in both Mtln knockout cell lines are shown in upper left corner. (B) Distributions of log2FC of TAGs in dependence on total number of double bonds. For lipidome experiment NIH3T3 ΔMtln-2,3 were analyzed.

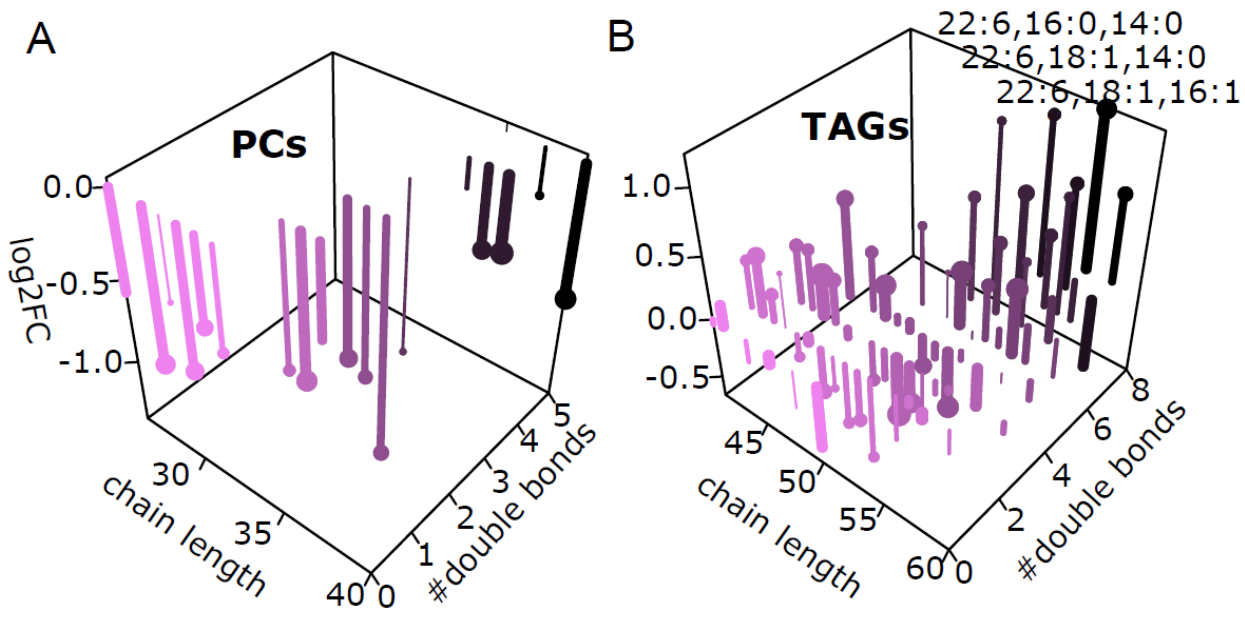

Fig. S12. Lipid concentration changes caused by disruption of Cyb5r3 mitochondrial localization (ΔCyb5r3$_{mito}$). Dependence of log2 fold change of PCs (A) or TAGs (B) in ΔCyb5r3$_{mito}$ (z-axis) on total chain length (x-axis) and number of double bonds (y-axis and color). Exact fatty chain composition is shown for three TAGs with highest fold change. Concentration of TAGs and PCs in wild type is shown by line width (in log scale). Lipids with statistically significant changes have a circle at the end of lines. Statistical significance was determined with Student's t-test (Benjamini-Hochberg-corrected p-value < 0.05).

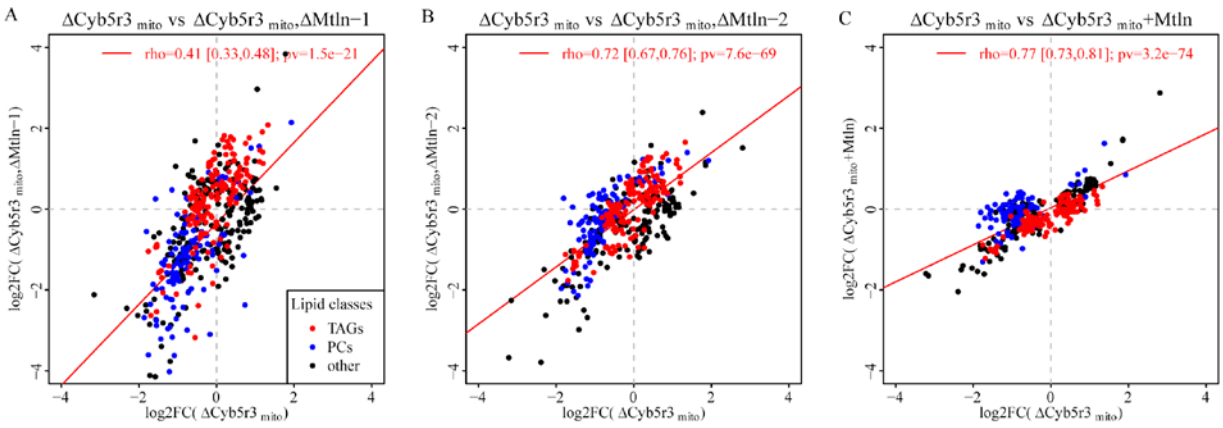

Fig. S13. Lipid concentration changes upon combined Cyb5r3 and Mtln mutations. Relationship between log2 fold lipid concentration changes induced by single $\Delta Cyb5r3_{mito}$ mutation (x-axis) and a combination of $\Delta Cyb5r3_{mito}$ mutation with two independent Mtln knockouts (A, B) or a combination of $\Delta Cyb5r3_{mito}$ mutation with Mtln overexpression (C) (y-axis). All log2 fold changes are relative to the parental wild type NIH3T3 cell line. Each point represents one lipid, triacylglycerols (TAG), glycerophosphates (GP), and other lipid classes are shown in red, blue, and black respectively.

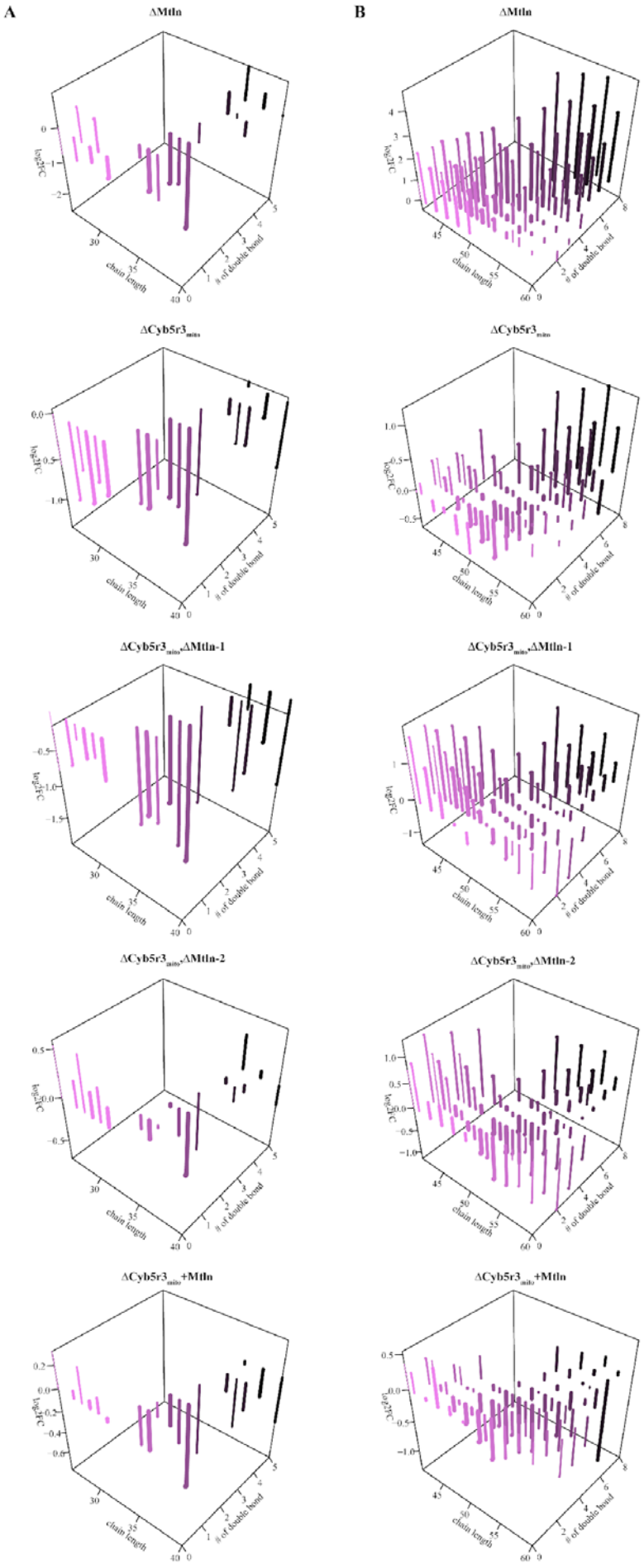
A
B
ΔMtln
ΔCyb5r3mito
ΔCyb5r3mito,ΔMtln-1
ΔCyb5r3mito,ΔMtln-2
ΔCyb5r3mito+Mtln
log2FC
chain length
# of double bond

Fig. S14. Concentration changes of PCs and TAGs upon combined Cyb5r3 and Mtln mutations. Dependence of log2 fold change of PCs (A) or TAGs (B) in ΔMtln-3, ΔCyb5r3$_{mito}$, ΔCyb5r3$_{mito}$,ΔMtln-1, ΔCyb5r3$_{mito}$,ΔMtln-2, ΔCyb5r3$_{mito}$+Mtln (z-axis) on total chain length (x-axis) and number of double bonds (y-axis and color). Concentration of TAGs and PCs in wild type is shown by line width (in log scale). Lipids with statistically significant changes have a circle at the end of lines. Statistical significance was determined with Student's t-test (Benjamini-Hochberg-corrected p-value < 0.05).

SUPPLEMENTARY REFERENCES

1. Ran FA, *et al.* (2013) Genome engineering using the CRISPR-Cas9 system. *Nat Protoc* 8(11):2281-2308.
2. Mates L, *et al.* (2009) Molecular evolution of a novel hyperactive Sleeping Beauty transposase enables robust stable gene transfer in vertebrates. *Nat Genet* 41(6):753-761.
3. Kowarz E, Loscher D, & Marschalek R (2015) Optimized Sleeping Beauty transposons rapidly generate stable transgenic cell lines. *Biotechnol J* 10(4):647-653.
4. Wojtala A, *et al.* (2014) Methods to monitor ROS production by fluorescence microscopy and fluorometry. *Methods Enzymol* 542:243-262.
5. Korshunov SS, Skulachev VP, Starkov AA. (1997) High protonic potential actuates a mechanism of production of reactive oxygen species in mitochondria. *FEBS Lett.* 1997 Oct 13;416(1):15-8.
6. Komlódi T, Sobotka O, Krumschnabel G, Bezuidenhout N, Hiller E, Doerrier C, Gnaiger E. (2018) Comparison of Mitochondrial Incubation Media for Measurement of Respiration and Hydrogen Peroxide Production. *Methods Mol Biol*. 1782:137-155
7. Rustin P, Chretien D, Bourgeron T, Gérard B, Rötig A, Saudubray JM, Munnich A. (1994) Biochemical and molecular investigations in respiratory chain deficiencies. *Clin Chim Acta* 228(1):35-51.
8. Zhang J, *et al.* (2012) Measuring energy metabolism in cultured cells, including human pluripotent stem cells and differentiated cells. *Nat Protoc* 7(6):1068-1085.
9. Sarafian MH, et al. (2014) Objective set of criteria for optimization of sample preparation procedures for ultra-high throughput untargeted blood plasma lipid profiling by ultra performance liquid chromatography-mass spectrometry. *Anal Chem* 86(12):5766-5774.
10. Ranninger C, et al. (2015) Nephron Toxicity Profiling via Untargeted Metabolome Analysis Employing a High Performance Liquid Chromatography-Mass Spectrometry-based Experimental and Computational Pipeline. *J Biol Chem* 290(31):19121-19132.
11. Bozek K, et al. (2015) Organization and evolution of brain lipidome revealed by large-scale analysis of human, chimpanzee, macaque, and mouse tissues. Neuron 85(4):695-702.
12. Libiseller G, et al. (2015) IPO: a tool for automated optimization of XCMS parameters. BMC Bioinformatics 16:118.
13. Benton HP, Want EJ, & Ebbels TM (2010) Correction of mass calibration gaps in liquid chromatography-mass spectrometry metabolomics data. Bioinformatics 26(19):2488-2489.
14. Smith CA, Want EJ, O'Maille G, Abagyan R, & Siuzdak G (2006) XCMS: processing mass spectrometry data for metabolite profiling using nonlinear peak alignment, matching, and identification. Anal Chem 78(3):779-787.
15. Tautenhahn R, Bottcher C, & Neumann S (2008) Highly sensitive feature detection for high resolution LC/MS. BMC Bioinformatics 9:504.
16. Kuhl C, Tautenhahn R, Bottcher C, Larson TR, & Neumann S (2012) CAMERA: an integrated strategy for compound spectra extraction and annotation of liquid chromatography/mass spectrometry data sets. Anal Chem 84(1):283-289.
17. Team RDC (2008) R: A language and environment for statistical computing. R Foundation for Statistical Computing.
18. Fahy E, et al. (2009) Update of the LIPID MAPS comprehensive classification system for lipids. J Lipid Res 50 Suppl:S9-14.
19. Blanchette M, *et al.* (2004) Aligning multiple genomic sequences with the threaded blockset aligner. *Genome Res* 14(4):708-715.
20. Michel AM, *et al.* (2014) GWIPS-viz: development of a ribo-seq genome browser. *Nucleic Acids Res* 42(Database issue):D859-864.